


RESEARCH ARTICLE

MRI evaluation of vulvar squamous-cell carcinoma in fresh radical local excision specimens for cancer localization and prediction of surgical tumor-free margins

Jan Heidkamp MS¹  | Petra L.M. Zusterzeel MD, PhD² |
Adriana C.H. van Engen-van Grunsven MD, PhD³ | Christiaan G. Overduin PhD¹ |
Andor Veltien BS¹ | Arie Maat³ | Maroeska M. Rovers PhD⁴ | Jurgen J. Fütterer MD, PhD¹

¹Department of Radiology and Nuclear Medicine, Radboud University Medical Center, Nijmegen, The Netherlands

²Department of Obstetrics and Gynaecology, Radboud University Medical Center, Nijmegen, The Netherlands

³Department of Pathology, Radboud University Medical Center, Nijmegen, The Netherlands

⁴Department of Operating Rooms, Radboud University Medical Center, Nijmegen, The Netherlands

Correspondence

Jan Heidkamp, Department of Radiology and Nuclear Medicine, Radboud University Medical Center, P.O. Box 9101, internal postal code 766, 6500 HB Nijmegen, The Netherlands.

Email: jan.heidkamp@radboudumc.nl

In the surgical treatment of vulvar squamous-cell carcinoma (VSCC), tumor-free margins of 8 mm or more are considered adequate. However, limited perioperative information on the tumor-free margins other than the surgeon's own estimation is available. The purpose of this study was therefore to investigate the feasibility of ex vivo MRI in localizing VSCC and to assess the surgical tumor-free margins in fresh radical local excision (RLE) specimens to guide the surgeon during resections. Nine patients with biopsy-proven VSCC scheduled for RLE were prospectively included. Intact fresh specimens were scanned using a 7 T preclinical MR-scanner. Whole mount H&E-stained slides were obtained every 3 mm and correlated with ex vivo MRI. A pathologist annotated VSCC and minimal tumor-free margins (3 o'clock, 9 o'clock, basal) on the digitalized histological slides. An observer with knowledge of histology (the non-blinded annotation) and a radiologist blinded to histology (the blinded annotation) separately performed annotation of the same features on ex vivo MRI. Linear correlation and agreement of the ex vivo MRI measurements with histology were assessed. Diagnostic performance for VSCC localization and identification of margins less than 8 mm was expressed as positive and negative predictive values (PPV, NPV). In 153 matched ex vivo MRI slices, the observer correctly identified 79/91 margins as less than 8 mm (PPV 87%) and 110/124 margins as 8 mm or greater (NPV 89%). The radiologist correctly annotated absence of VSCC in 73/81 (NPV 90%) and presence in 65/72 (PPV 90%) slices. Sixty-four of 90 margins were correctly identified as less than 8 mm (PPV 71%) and 83/102 margins as 8 mm or greater (NPV 81%). Both non-blinded and blinded annotations were linearly correlated and demonstrated good agreement with histology. Accurate localization of VSCC and measurements of the surgical tumor-free margins in fresh RLE specimens using ex vivo MRI seems feasible. High diagnostic performance in VSCC localization and identification of margins less than 8 mm suggest ex vivo MRI to be clinically applicable.

KEYWORDS

margins of excision, MRI, vulvar neoplasms, whole mount histology

This is an open access article under the terms of the Creative Commons Attribution-NonCommercial-NoDerivs License, which permits use and distribution in any medium, provided the original work is properly cited, the use is non-commercial and no modifications or adaptations are made.

© 2018 The Authors. *NMR in Biomedicine* published by John Wiley & Sons Ltd.

1 | INTRODUCTION

Vulvar cancer is the fourth most common gynecologic cancer, accounting for approximately 5% of all malignancies of the female genital tract and typically occurs in women aged 70 and above.¹⁻³ Among the several histological types, squamous-cell carcinomas constitute the majority (90%).⁴

Historically, patients were treated with radical vulvectomy including “en bloc” bilateral inguino-femoral and pelvic lymphadenectomy.^{5,6} The corresponding 5 year survival rate was 75%, but due to the extensive nature of this operation it was also associated with severe postoperative complications such as wound breakdown, infection, lymphedema, and psychosexual disturbance.⁷⁻¹⁰ In order to avoid this morbidity, radical vulvectomy has been replaced by less extensive radical local excision (RLE) with inguinal lymph node dissection via separable incisions or a sentinel node procedure. This operation is as effective as radical vulvectomy in preventing local recurrences (LRs) and is currently the preferred treatment in early stage disease.^{6,11-14}

The most important predictive factor for LR is histological tumor-free margins of at least 8 mm.¹⁵⁻¹⁸ In order to achieve this, surgical margins of 10 mm,^{15,17,19} or even 20 mm, are recommended.¹⁶

The main challenge in treating vulvar squamous-cell carcinoma (VSCC) is therefore to keep surgical margins large enough to minimize the chance of LR, while simultaneously preserving as much genital tissue as possible to diminish morbidity to the urethra, clitoris or anal sphincter. The surgeon is, however, hampered by the fact that accurate and topical information regarding the margins is limited during or directly after the surgery. Frozen section analysis (FSA) is able to provide histological information, but may be prone to sampling error. Currently, both the surgeon and patient have to wait several days for the results of the histological analysis to determine the definitive margin status of the RLE. In the case of histological margins less than 8 mm, which may occur in approximately 40% of patients,¹⁸ re-excision or adjuvant radiotherapy is recommended.^{6,20}

We hypothesize that ex vivo MRI might provide additional three-dimensional volumetric information on the margin status of fresh RLE specimens, which may potentially allow accurate margin assessment within the perioperative time frame. Therefore, the aim of this pilot study was to assess the feasibility of ex vivo MRI in localizing VSCC and assessing the tumor-free margins in fresh RLE specimens to guide the surgeon during surgical resections.

2 | MATERIALS AND METHODS

2.1 | Study population

Prior to conducting the study, approval of our institutional review board and written informed consent from all patients were obtained. Patients with biopsy-proven VSCC and scheduled for RLE with either inguinal lymph node dissection or a sentinel node procedure were prospectively included. Patients scheduled for RLE because of recurrent VSCC were excluded.

2.2 | Preparation of the specimen

Directly after surgery, the intact RLE specimen was transported to the pathology department where the resection surface was inked and positioned in an in-house designed container (Figure 1). The specimens were positioned in such a way that a corresponding orientation between the ex vivo MRI and histological slicing was achieved.

2.3 | Ex vivo MRI acquisition

The specimen was immersed in perfluoropolyether (PFPE) (Galden, Solvay Solexis, Thorofare, NJ, USA) to eliminate potential magnetic susceptibility artifacts arising at the air-tissue transition and scanned using a 7 T horizontal 154 mm wide bore MRI system (ClinScan, Bruker BioSpin, Ettlingen, Germany), interfaced to a Siemens console (Syngo MR B15, Siemens Healthcare, Erlangen, Germany). An integrated circular polarized transmit/receive ¹H volume coil acquired the images. Axial fast low-angle shot (FLASH) T_1 -weighted (T_1W), turbo spin echo (TSE) and half-Fourier acquisition single-shot TSE (HASTE) diffusion weighted (DW) images were acquired. The TSE images were acquired using echo times (T_E) of 13 (TSE-13), 26 (TSE-26), and 53 (TSE-53) ms. Furthermore, TSE images with higher spatial resolution (TSE HR) were acquired. The diffusion sensitizing gradient was the same as the slice selection gradient. Using a double bipolar pulsed field gradient spin echo sequence with PFG durations of 4.25 ms and spacing between two PFGs of 5.2 ms b -values of 0, 100, 500, 1000, and 1200 s/mm² were obtained. The apparent diffusion coefficient (ADC) maps were calculated using the standard ADC post processing of Syngo B15. The number of contiguous slices was chosen to completely cover the specimen (Table 1).

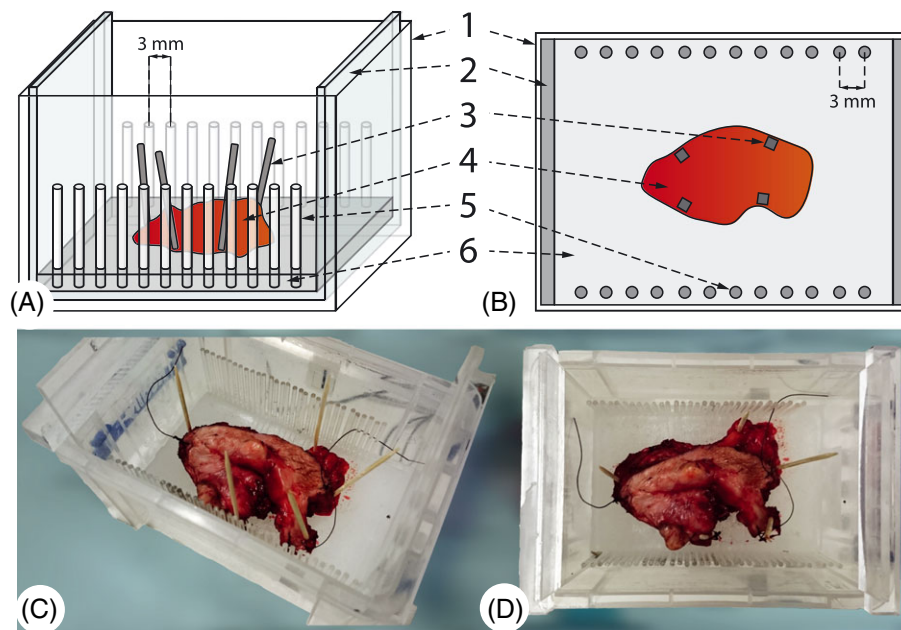


FIGURE 1 The in-house designed container used to hold the RLE specimens during ex vivo MRI acquisition enabled correlation between the ex vivo MRI slices and histological slides. A, B, Schematic representations of the container as viewed from the front and above respectively, showing the outer box (1) holding a Perspex insert (2) on which a layer of paraffin (6) was molded. The specimens (4) were pinned down on the paraffin layer using wooden pins (3). The two rows of opposing rods (5) standing at 3 mm intervals were used by the pathologist for accurate specimen slicing with high reproducibility of the thickness and orientation of the sections so that the correlation with ex vivo MRI was as accurate as possible. C, D, Slight oblique/top and top view respectively of an example of an RLE specimen obtained from a 93-year-old patient. Sutures were applied to demarcate the 12 o'clock side of the specimen and the position at which the specimen was transected for surgical resection purposes

TABLE 1 MRI sequence parameters

Sequence	No of slices (min-max)	T_R (ms)	T_E (ms)	FA (degrees)	ST (mm)	NSA	Voxel size (mm)	Matrix	Scan time (m:s)	Echo train length	Readout bandwidth (Hz/Px)
T1W FLASH	40–82	400	3	40	1	1	0.31	256 × 256	01:23	n/a	400
TSE-13, TSE-26, TSE-53	40–82	6 090–12 470	13, 26, 53	180	1	1	0.31	256 × 256	03:40–07:30	7	130
TSE HR	40–82	6 400–13 120	14	180	1	1	0.16	512 × 512	07:49–16:01	7	130
DWI HASTE ^a	40–82	2 130	53	180	1	4	0.63	128 × 128	05:41–11:39	n/a	425

FA, flip angle; ST, slice thickness; NSA, number of signal averages; n/a, not applicable.

^a b -values of 0, 100, 500, 1000, and 1200 s/mm² were acquired; from these the ADC maps were calculated.

2.4 | Histological processing

Following ex vivo MRI acquisition, the container with the RLE specimen was returned to the pathology laboratory. After formalin fixation, the specimen was completely cut into 3 mm thick slices, for which the opposing rows of rods directed the slice orientation and thickness. From each of the 3 mm whole mount paraffin embedded slices a 4 μ m hematoxylin and eosin stained slice was obtained and microscopically examined. Subsequently, the histological slides were digitalized using a XC10 color camera attached to a BX51 bright field microscope (both Olympus Corporation, Tokyo, Japan) for the mega-sized slides, and a Panoramic 250 Flash III (3DHISTECH, Budapest, Hungary) fully automatic digital microscope for the regular sized slides. A pathologist (Ave, 7 years' experience in gynecopathology), unaware of the ex vivo MRI, measured the height (epidermis-basal margin) and width (left–right) of the specimens on the middlemost slide using CaseViewer v2.0 (3DHISTECH). VSCC location, both minimal lateral margins (3 and 9 o'clock), and minimal basal margin were annotated and used for analysis, whereas the craniocaudal margins (12 and 6 o'clock) were annotated but not used for analysis. Furthermore, the linear extension, invasion depth, and FIGO and TNM stage were reported. Finally, the pathologist reported that the ex vivo MRI examination did not cause any changes to the RLE specimens and it did not adversely affect normal clinical reporting.

2.5 | Qualitative image evaluation

A radiologist (JF, 8 years experience in genitourinary imaging), unaware of the histology, performed qualitative analysis of the general image quality for seven ex vivo MRI series: T1W, TSE-13, TSE-26, TSE-53, TSE HR, ADC map and diffusion weighted imaging (DWI) with a b -value of 1000 s/mm^2 ($b1000$). The following five-point rating scale was used²¹: 1, very bad non-diagnostic quality images; 2, low image quality that degraded confidence in diagnosis; 3, moderate image quality sufficient for diagnosis; 4, good image quality; 5, excellent image quality enabling visualization of even small structures. Furthermore, the visibility of the tumor and the transition between the epidermis and the resection surface, i.e. the point in the epidermis where the surgeon started excising the tissue creating a resection surface, were assessed using the following scale: 1, very poor; 2, poor; 3, sufficient; 4, good; 5, excellent.

2.6 | Ex vivo MRI evaluation

A non-blinded observer (JH) directly matched the best scoring MRI series in the qualitative image evaluation with histology. Individual MRI slices were roughly correlated with digitalized histological slides by matching every third 1 mm thick MRI slice to a histological slide obtained every 3 mm of the specimen, starting from the first tissue containing MRI slice. A further precise match was performed using the contours of the specimen and anatomical landmarks. The height and width of the specimen were measured on ex vivo MRI on the matching middlemost slice at identical positions as on the histological slide and directly compared with histology to calculate the formalin fixation induced shrinkage factor. To investigate technical feasibility of ex vivo MRI in localizing VSCC and assessing the tumor-free margins, the observer annotated the VSCC boundaries and minimal surgical tumor-free margins (3 and 9 o'clock, and basal) on ex vivo MRI using a dedicated workstation developed in MATLAB R2014b (MathWorks, Natick, MA, USA) which was simultaneously displayed with the histological slides. This will be referred to as the non-blinded annotation. Subsequently, to investigate clinical applicability of ex vivo MRI a radiologist (JF) independently performed annotation of the same features, but unaware of histology (the blinded annotation). The actual annotations were made only on MRI series that obtained the highest score in the qualitative evaluation, the rest of the series were used at the readers' own discretion to obtain additional information.

2.7 | Statistical analysis

Descriptive statistics were performed, i.e. medians and interquartile ranges were calculated. Both ex vivo MRI annotations were corrected for formalin fixation induced shrinkage with the mean shrinkage factor. To determine the correlation between histology, and the non-blinded and blinded annotations, Spearman's correlation coefficients were calculated and Bland-Altman analysis was performed to assess the agreement. Based on the non-blinded annotation, positive and negative predictive values (PPV NPV) as well as sensitivity and specificity were calculated to assess the diagnostic performance of ex vivo MRI in identifying margins less than 8 mm. Based on the blinded annotation the diagnostic performance of ex vivo MRI was determined in both localizing VSCC and identifying margins less than 8 mm. The diagnostic performance in identifying margins less than 8 mm was calculated using two approaches: one that omitted the false negative VSCC cases from the calculation (optimistic approach) and one that included the false negative VSCC cases (conservative approach). Correct annotation of VSCC presence and correct identification of a less than 8 mm margin were considered true positives, while correct annotation of VSCC absence and correct identification of an 8 mm or greater margin were considered true negatives. For the conservative approach, both margins less than 8 mm, and 8 mm or greater, that were not evaluated as a result of missed VSCC cases were considered as false negatives. The performance of the blinded reader in identifying less than 8 mm margins was analyzed using receiver operating characteristic (ROC) analysis and the area under the curve (AUC) was calculated. The optimal margin cut-off value which potentially yields maximum effectiveness of ex vivo MRI was determined by calculating the Youden index (J) which is the maximum vertical distance between the ROC curve and the chance line.²² The Dice similarity coefficient (DSC) was calculated to determine the spatial overlap between the VSCC area of both annotations on ex vivo MRI, with $DSC = 0$ indicating no overlap; and $DSC = 1$ indicating complete overlap.²³

3 | RESULTS

In total nine patients were included between March and September 2015 (Table 2). Of nine specimens, 156 histological slides were obtained, of which 72 contained VSCC including three slides containing two separate VSCC lesions each, resulting in a total of 75 areas of VSCC. Histology annotated 74 areas of VSCC due to one excluded slide, in which the tumor was dislodged from rest of the tissue. Furthermore, 73, 73 and 74 annotations of the 3 o'clock, 9 o'clock and basal margins were made. In one case the 3 o'clock and 9 o'clock margins could not be determined due to incomplete histological slicing.

TABLE 2 Clinical and histological characteristics of study cohort ($n = 9$)

Characteristics	Value (%)
Age (y)	81 (58–93) ^a
BMI	26.3 (20.5–31.1) ^a
SNP	6 (66)
ILND	1 (11)
LVSI	3 (33)
Linear extension (mm)	15 (1–46) ^a
Invasion depth (mm)	2.5 (0.7–15) ^a
Minimal tumor-free margin (mm)	8 (2.5–14) ^a
FIGO stage	
1A	1 (11)
1B	7 (78)
3A	1 (11)

SNP, sentinel node procedure; ILND, inguinal lymph node dissection; SCC, squamous cell carcinoma; LVSI, lymphovascular space invasion.

^aMedian value with range between parentheses.

3.1 | Qualitative image evaluation

Overall, the TSE series, particularly the TSE HR series, demonstrated the highest median scores for all three features (Figure 2). The scores were independent of the T_E used, except for the visibility of the epidermis-resection edge transition, which was assigned a lower median score at TSE-53. Consequently, the TSE HR series were used for annotations. The b1000 series and the ADC map scored a *good* for tumor visualization (both median 4), yet visualization of the epidermis-resection edge transition was *very poor* (both median 1). Although the T1W series provided *good image quality* (median 4), it did not perform as well in visualization of the tumor (median 3) or epidermis-resection edge transition (median 1.5).

3.2 | Ex vivo MRI evaluation

Of the 156 histological slides, 153 were correlated to ex vivo MRI (Figure 3). Three non-tumor-containing histological slides from the edges of the specimen were not correlated, as these were not covered by MRI. The mean formalin fixation induced shrinkage factor was 23% (95% confidence interval (95% CI) 16%–29%); the margin annotations on ex vivo MRI were therefore corrected by a factor of 0.77 and the two-dimensional VSCC-area annotations by a factor of 0.59 (0.77 squared).

In the non-blinded annotations (Figures 4 and 5), VSCC was annotated in 73 of the 153 correlated MRI slices. One VSCC area (0.5 mm²) on histology was not localized on ex vivo MRI, which precluded margin annotations. Furthermore, 70, 72 and 73 annotations of 3 o'clock, 9 o'clock and basal margins were made. Four margin annotations were excluded due to the specimen surfacing above the PFPE, causing magnetic susceptibility artifacts, which precluded reliable measurements. Seventy-nine out of 91 margins less than 8 mm were in agreement with histology (PPV

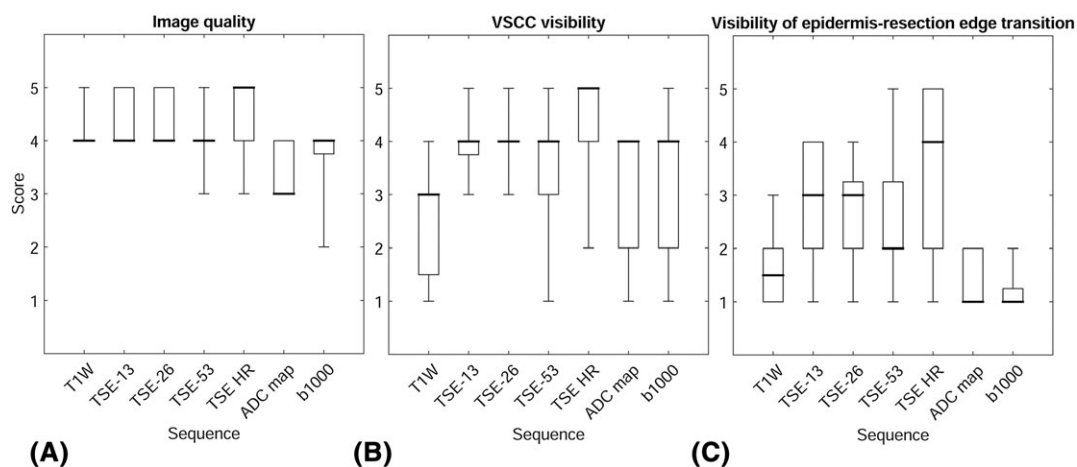


FIGURE 2 Box-whisker plots showing the results of the qualitative image evaluation with the results for image quality (A), VSCC visibility (B) and visibility of the epidermis-resection edge transition (C). The box plots demonstrate the median score (bold horizontal lines), interquartile range (boxes) and extreme values (whiskers). Overall, the TSE HR series obtained the highest scores during the qualitative image evaluation

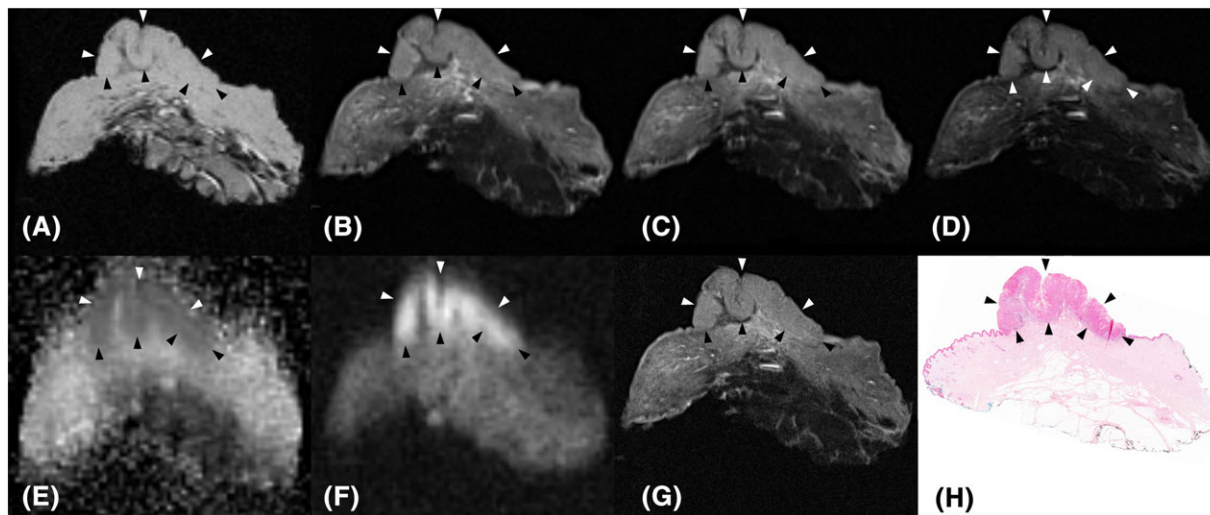


FIGURE 3 Ex vivo MRI and corresponding histology acquired from a fresh RLE specimen of the vulva obtained from a 75-year-old patient. A, A T1W image that provided limited contrast between the tumor and surrounding tissue; as a result it was only vaguely visible (white and black arrow heads). B-D, TSE images acquired using different T_E values of 13, 27 and 54 ms respectively. With increasing T_E the contrast between the tumor (white and black arrow heads) and healthy tissue appears to increase, but at the expense of the amount of signal obtained. E, F, DW images constituting an ADC map (E) and a b1000 image (F) on which the tumor (white and black arrow heads) is easily spotted. The images were not suitable for accurate tumor delineation and tumor-free margin assessment as a result of a lower resolution. G, TSE image with $T_E = 14$ ms and higher resolution compared with B-D (voxel size = 0.16×0.16 mm versus 0.31×0.31 mm), which provided high anatomical detail that was advantageous for tumor (white and black arrow heads) delineation. H, The corresponding hematoxylin and eosin stained histological slide at 100 \times magnification confirmed a FIGO stage 3A VSCC (black arrow heads)

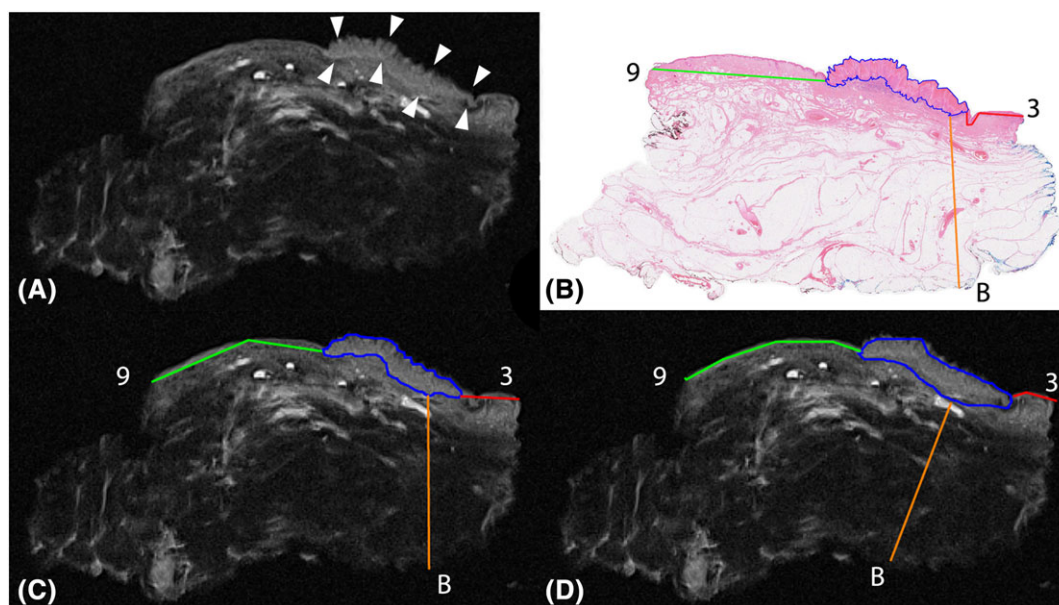


FIGURE 4 Example of VSCC and surgical margin annotation on ex vivo MRI (TSE HR, $T_R/T_E = 10\ 240/14$ ms) and histological slide obtained from an RLE specimen from an 81-year-old patient. A, Non-annotated ex vivo MRI with the VSCC indicated (white arrow heads) for reference. B, The corresponding hematoxylin and eosin stained histological slide at 100 \times magnification confirmed a FIGO stage 1B VSCC (area = $14.3\ \text{mm}^2$), which is demarcated by the solid blue line. Furthermore, 3 o'clock (3)-, 9 o'clock (9)- and basal (B) margins of 5.3, 12.1 and 12.1 mm were annotated respectively. C, Non-blinded annotation of VSCC (solid blue line) with an area of $16.0\ \text{mm}^2$ and 3 o'clock-, 9 o'clock- and basal margins of 4.3, 13.4 and 12.9 mm (all shrinkage corrected) respectively. D, Blinded annotation by the radiologist, who found a VSCC area of $22.3\ \text{mm}^2$ and 3 o'clock-, 9 o'clock- and basal margins of 3.2, 13.8 and 12.6 mm. The DSC of the non-blinded and blinded annotations of VSCC area was 0.75. The blinded annotator identified correctly categorized all three margins as either less than 8 mm, or 8 mm or greater

87%; 95% CI 80%–93%). The NPV was 89% (95% CI 83%–94%), i.e. 110 out of 124 margins of 8 mm or greater were correctly identified with ex vivo MRI (Table 3). The non-blinded VSCC-area annotations showed a positive correlation with histology (0.96 , $p < 0.01$). The correlations for the 3 o'clock, 9 o'clock and basal margins were 0.87 ($p < 0.01$), 0.80 ($p < 0.01$) and 0.89 ($p < 0.01$) (Figure 6). Bland-Altman analysis

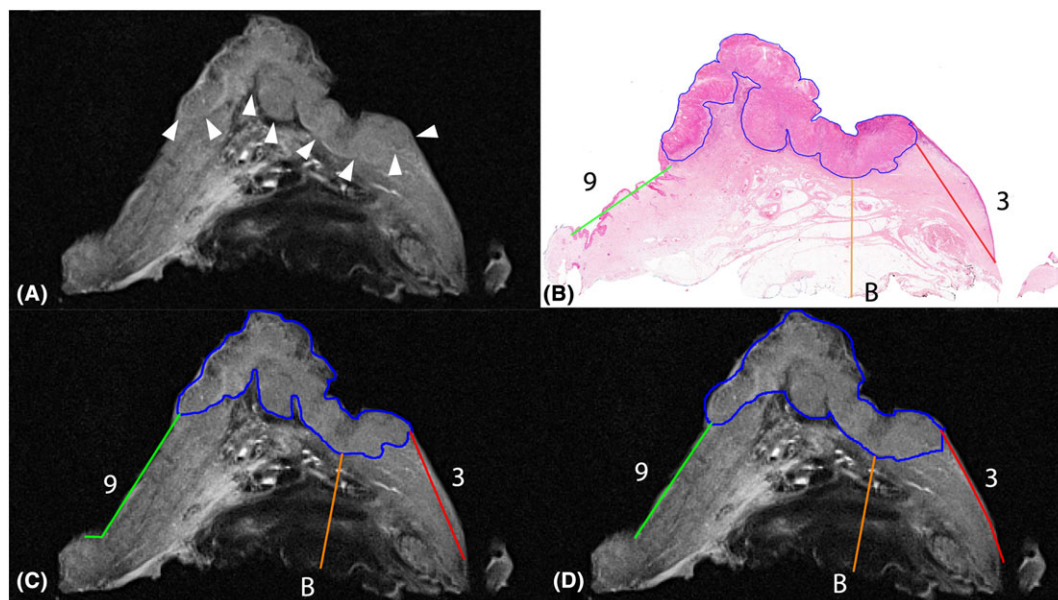


FIGURE 5 Example of VSCC and surgical margin annotation on ex vivo MRI (TSE HR, $T_R/T_E = 10\ 240/14$ ms) and histological slide obtained from an RLE specimen from an 75-year-old patient. A, Non-annotated ex vivo MRI on which the VSCC is indicated (white arrow heads) for reference. B, The corresponding hematoxylin and eosin stained histological side at 100 \times magnification confirmed a FIGO stage 3A VSCC (area = 65.6 mm²) demarcated by the solid blue line. Furthermore, 3 o'clock (3)-, 9 o'clock (9)- and basal (B) margins of 9.2, 7.7 and 7.6 mm were annotated respectively. C, Non-blinded annotation of VSCC (solid blue line) with an area of 77.9 mm² and 3 o'clock-, 9 o'clock- and basal margins of 12.2, 13.6 and 8.8 mm (all shrinkage corrected) respectively. D, Blinded annotation by the radiologist, who found a VSCC area of 84.3 mm² and 3 o'clock-, 9 o'clock- and basal margins of 11.1, 10.6 and 8.8 mm. The DSC of the non-blinded and blinded annotations of VSCC area was 0.93. Both the non-blinded and blinded annotators correctly identified the 8 mm or greater 3 o'clock margin, but failed to identify the less than 8 mm 9 o'clock and basal margins. Since the start and end positions of the margin measurements appear to be positioned correctly, the discrepancy seems to be caused by tissue floating on the Galden, resulting in tissue deformation. Note the parachute-like shape of the specimen on ex vivo MRI compared with the histological image

TABLE 3 PPV and NPV, and sensitivity and specificity of ex vivo MRI in identifying margins less than 8 mm after non-blinded annotation stratified by margin location

	3 o'clock margin	9 o'clock margin	Basal margin	Margins combined
<8 mm, n/N (PPV, 95% CI)	30/36 (0.83, 0.71–0.96)	13/15 (0.87, 0.69–1.0)	36/40 (0.90, 0.81–0.99)	79/91 (0.87, 0.80–0.94)
\geq 8 mm, n/N (NPV, 95% CI)	30/34 (0.88, 0.77–0.99)	53/57 (0.93, 0.86–1.0)	27/33 (0.82, 0.69–0.95)	110/124 (0.89, 0.83–0.94)
<8 mm, n/N (sensitivity, 95% CI)	30/34 (0.88, 0.77–0.99)	13/17 (0.76, 0.56–0.97)	36/42 (0.86, 0.75–0.96)	79/93 (0.85, 0.78–0.92)
\geq 8 mm, n/N (specificity, 95% CI)	30/36 (0.83, 0.71–0.96)	53/55 (0.96, 0.91–1.0)	27/31 (0.87, 0.75–0.99)	110/122 (0.90, 0.85–0.95)

demonstrated a mean difference (bias) between ex vivo MRI and histology of the VSCC area of 4.8 mm². This overestimation appeared to be driven by the larger positive differences between ex vivo MRI and histology at larger mean VSCC areas. Bland–Altman analysis for the 3 o'clock, 9 o'clock and basal margins demonstrated biases of 0.0, 0.4 and 0.2 mm and no clear trend for margin size (Figure 6).

In the blinded annotations (Figures 4 and 5), absence of VSCC was annotated in 81 ex vivo MRI slices, of which 73 were in agreement with histology (NPV 90%; 95% CI 84%–97%). Presence of VSCC was correctly annotated in 65 out of 72 slices (PPV 90%; 95% CI 83%–97%). The sensitivity and specificity were 89% (95% CI 82%–96%) and 91% (95% CI 85%–97%). In the 65 true positive VSCC slices, 90 margins were identified as less than 8 mm and 102 as 8 mm or greater, of which 64 (PPV 71%; 95% CI 62%–80%) and 83 (NPV 81%; 95% CI 74%–89%) corresponded with histology, respectively (Table 4). In the conservative approach (Table 4), eight false negative VSCC slices were included so that 83 out of 125 margins of 8 mm or greater corresponded with histology, which decreased the NPV to 66% (95% CI 58%–75%). By including the false negative VSCC slices, eight 9 o'clock and basal margin annotations and seven 3 o'clock margin annotations (one false negative VSCC slice contained a 3 o'clock margin annotation that was excluded) were added consisting of three, six and two margins of less than 8 mm respectively. The blinded VSCC-area annotation showed a positive correlation with histology (0.93, $p < 0.01$), which was comparable with the non-blinded annotation. Furthermore, the 3 o'clock, 9 o'clock and basal margins showed correlations of 0.52 ($p < 0.01$), 0.54 ($p < 0.01$) and 0.62 ($p < 0.01$) (Figure 7). These correlations were less strong than for the non-blinded annotation. Bland–Altman analysis revealed a mean overestimation of the VSCC area (14.7 mm²) by the blinded annotation, which is larger as compared with the non-blinded annotation (4.8 mm²). Analogously to the non-blinded annotation, this overestimation appeared to be driven by the relatively larger positive differences between ex vivo MRI and

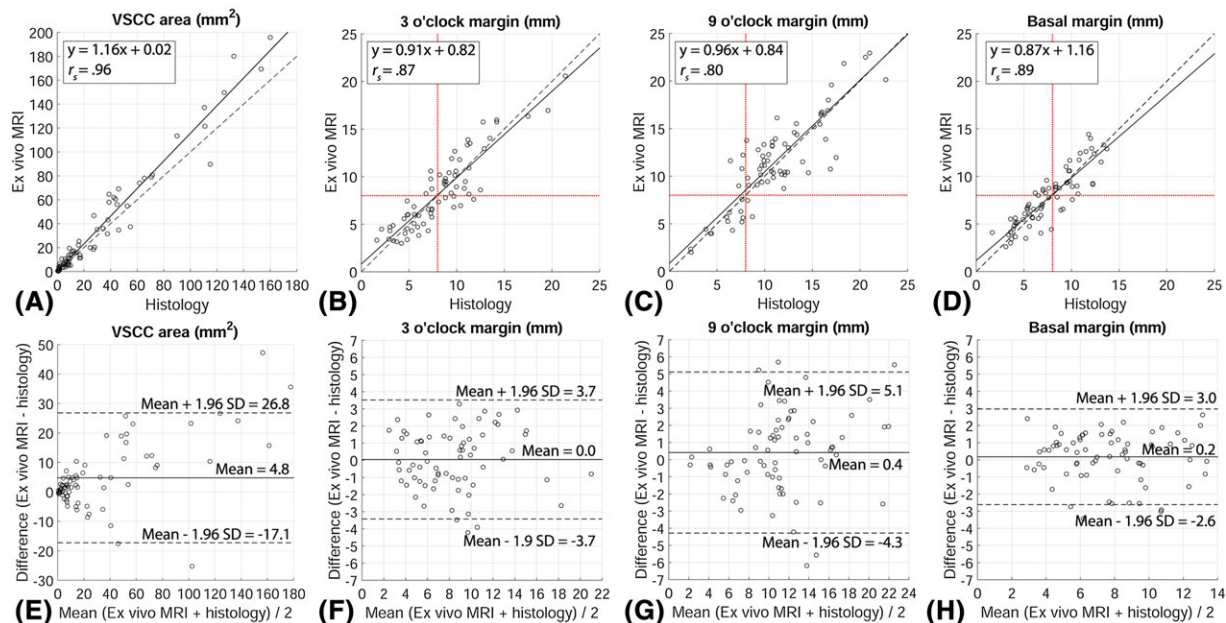


FIGURE 6 For the non-blinded annotation, scatter plots (A-D) and Bland–Altman plots (E-H) showing the linear correlation and agreement between the variables measured on histology and ex vivo MRI. A, E, The VSCC-area variable; B-D, F-H, the 3 o'clock, 9 o'clock and basal margin variables respectively. A-D, Linear regression equation, Spearman's rank correlation coefficient (r_s), regression line (solid line), unity line (dashed line) and two reference lines at 8 mm cut-off (red dotted lines) are provided as reference. E, F, Mean difference (solid line) and 95% limits of agreement (dashed lines) are provided as reference. SD, standard deviation

TABLE 4 PPV and NPV, and sensitivity and specificity of ex vivo MRI in identifying margins less than 8 mm after blinded annotation using an optimistic approach that excluded the false negative VSCC slices ($n = 8$) and a conservative approach that included them.

	False negative VSCC slices excluded				False negative VSCC slices ($n = 8$) included			
	3 o'clock margin	9 o'clock margin	Basal margin	Margins combined	3 o'clock margin	9 o'clock margin	Basal margin	Margins combined
<8 mm, n/N (PPV, 95% CI)	21/33 (0.64, 0.47–0.80)	10/13 (0.77, 0.54–1.0)	33/44 (0.75, 0.62–0.88)	64/90 (0.71, 0.61–0.80)	21/33 (0.64, 0.47–0.80)	10/13 (0.77, 0.54–1.0)	33/44 (0.75, 0.62–0.88)	64/90 (0.71, 0.61–0.80)
≥ 8 mm, n/N (NPV, 95% CI)	19/30 (0.63, 0.46–0.81)	46/51 (0.90, 0.82–0.82)	18/21 (0.86, 0.70–1.0)	83/102 (0.81, 0.74–0.89)	19/37 (0.51, 0.35–0.67)	46/59 (0.78, 0.67–0.89)	18/29 (0.62, 0.44–0.80)	83/125 (0.67, 0.58–0.75)
<8 mm, n/N (sensitivity, 95% CI)	21/32 (0.66, 0.49–0.82)	10/15 (0.67, 0.43–0.91)	33/36 (0.92, 0.82–1.0)	64/83 (0.77, 0.68–0.86)	21/39 (0.54, 0.38–0.69)	10/23 (0.43, 0.23–0.64)	33/44 (0.79, 0.66–0.91)	64/106 (0.60, 0.51–0.70)
≥ 8 mm, n/N (specificity, 95% CI)	19/31 (0.61, 0.44–0.78)	46/49 (0.94, 0.87–1.0)	18/29 (0.62, 0.44–0.79)	83/109 (0.76, 0.68–0.84)	19/31 (0.61, 0.44–0.78)	46/49 (0.94, 0.87–1.0)	18/29 (0.62, 0.44–0.79)	83/109 (0.76, 0.68–0.84)

histology at larger mean VSCC areas. Bland–Altman analysis of blinded annotation showed mean agreements with histology of 0.2 mm, 0.1 mm and -0.7 mm for the 3 o'clock, 9 o'clock and basal margins, respectively. There was no apparent trend for margin size (Figure 7). Bland–Altman analysis demonstrated wider 95% limits of agreement in the blinded annotation than in the non-blinded annotation, indicating less agreement.

ROC analysis of the performance of the blind reader in identifying less than 8 mm margins using ex vivo MRI yielded an AUC of 0.83 (95% CI 0.78–0.89). The optimal margin cut-off value of 7.3 mm was determined on the basis of the Youden index value of 0.58, yielding a sensitivity and specificity of 75% and 83% respectively (Figure 8).

Assessment of the spatial overlap between the VSCC area of both annotations on ex vivo MRI resulted in a DSC of 0.73 (95% CI 0.69–0.77).

4 | DISCUSSION

Our results demonstrated high diagnostic performance in VSCC localization and identification of less than 8 mm margins in fresh RLE specimens. Together with the high correlation and agreement between the blinded annotations and histology, this suggested clinical applicability. The high correlation and agreement of the non-blinded annotations demonstrated technical feasibility. The qualitative image evaluation showed high scores for the TSE sequences in general and for the DW sequences for VSCC visibility specifically, suggesting that these two combined constitute the optimal imaging protocol.

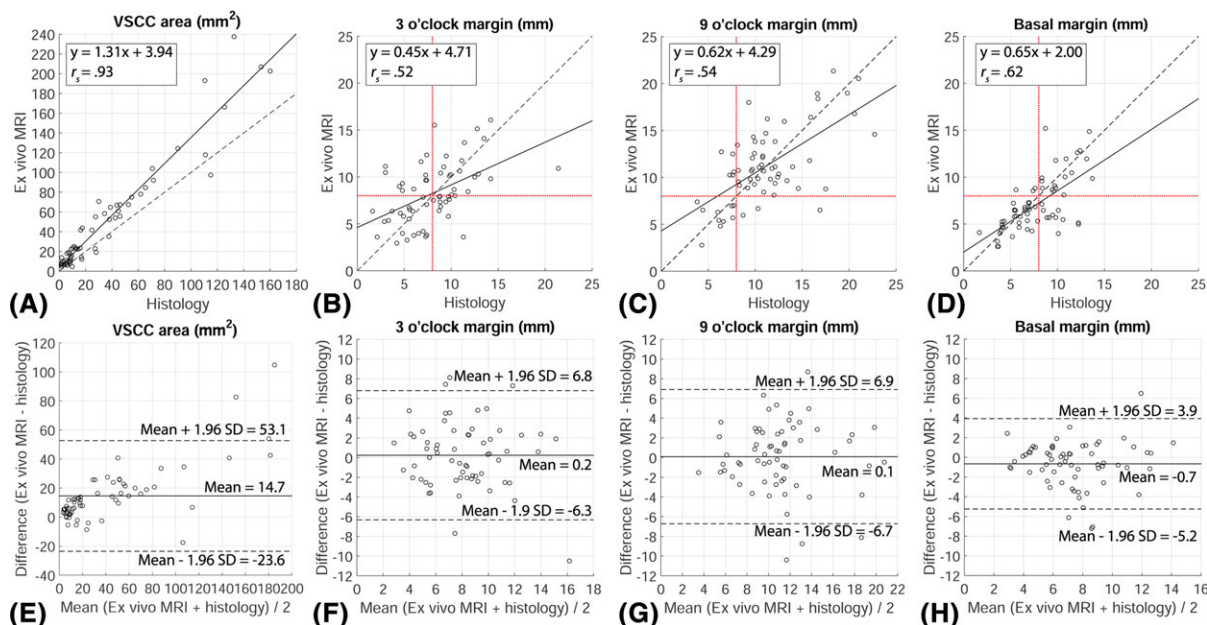


FIGURE 7 For the blinded annotation, scatter plots (A-D) and Bland–Altman plots (E-H) showing the linear correlation and agreement between the variables measured on histology and ex vivo MRI. A, E, The VSCC-area variable; B-D, F-H, the 3 o'clock, 9 o'clock and basal margin variables respectively. A-D, Linear regression equation, Spearman's rank correlation coefficient (r_s), regression line (solid line), unity line (dashed line) and two reference lines at 8 mm cut-off (red dotted lines) are provided as reference. E, F, Mean difference (solid line) and 95% limits of agreement (dashed lines) are provided as reference. SD, standard deviation

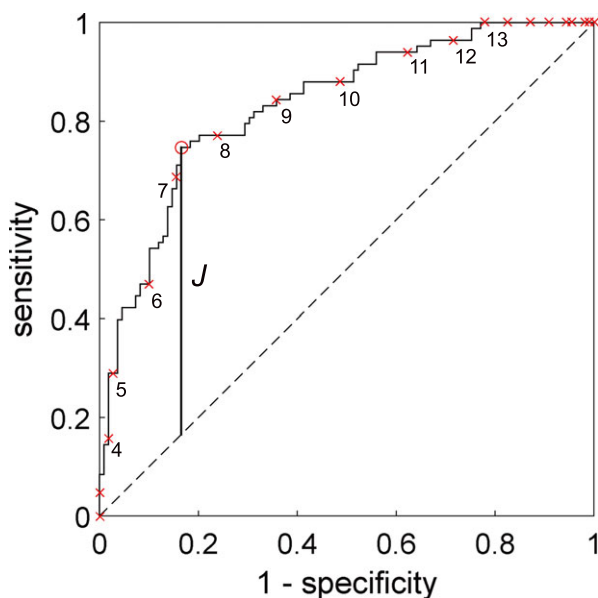


FIGURE 8 Plot of ROC curve of ex vivo MRI margin cut-off values for differentiating between tumor-free margins less than 8 mm and 8 mm or greater. The AUC was 0.83 (95% CI 0.78–0.89). Using the Youden index ($J = 0.58$) the optimal margin cut-off value was determined at 7.3 mm, yielding a sensitivity of 0.75 and a specificity of 0.83 (1 – specificity = 0.17). This point is demarcated by the red circle. The red crosses indicate the integer margin cut-off values

Several authors have pursued similar methods in an effort to provide surgeons with accurate perioperative information on the margin status in tumors other than VSCC. Previously, breast,^{24–26} bone,²⁷ gastric,²⁸ esophageal,²⁹ tongue³⁰ and prostate^{31,32} specimens have been examined by ex vivo MRI. As far as we are aware, employing ex vivo MRI in RLE specimens is new, but other (imaging) techniques such as FSA³³ and optical coherence tomography (OCT)³⁴ have been investigated as a means to assess the surgical tumor-free margins. Ex vivo MRI advantageously enables sampling of the surgical tumor-free margins of a cross section of the specimen every millimeter, whereas in FSA the number of samples remains limited. Application of OCT in RLE specimens might be limited due to the inadequate probing depth, which is typically about 2 mm. The formalin fixated shrinkage factor of 23% corresponded to previous findings of 20% and 25%.^{15,19}

Our results justify future investigations to further improve our method. Despite correction for the formalin fixation induced shrinkage factor, the non-blinded annotation demonstrated under- and overestimation of ex vivo MRI where one would theoretically expect none. This was

probably caused by differences between the shrinkages of the individual specimens and the calculated mean shrinkage factor. Besides that, both local tissue deformation caused by floating as a result of suboptimal mounting of the specimen on the paraffin layer as well as formalin fixation induced deformation might also have hampered the accuracy of the annotations in some cases. Likewise, these issues affected the blinded annotations even more strongly, as the scatter plots demonstrated more outliers (hence a weaker correlation with histology), wider limits of agreement and lower PPV and NPV for less than 8 mm margin identification compared with the non-blinded annotations. In measuring the tumor-free margins, the non-blinded reader was probably able to consider tissue deformation, whereas the blinded reader without knowledge of histology was not. Furthermore, difficulties in determining the transition between the epidermis and the resection surface might constitute another hampering factor. The relatively low scores for visibility of this feature in the qualitative image evaluation confirm this suspicion. Finally, the blinded reader was a novice in reading MRI of RLE specimens.

The strengths of our study comprise the gold standard of whole mount histological slides obtained from the RLE specimens every 3 mm rather than the one slide obtained according to protocol at the position where the narrowest margin is presumed. Furthermore, the separate non-blinded and blinded annotations of the ex vivo MRI disentangled the technical performance of ex vivo MRI from the performance of the blinded reader.

Some potential limitations, which might be attributed to the fact that this was a pilot study, should be discussed. First, the blinded annotation of ex vivo MRI was performed by a single reader only, which limits the reproducibility of the results. Second, the applied MRI protocol could take up to 1.5 h in case of large specimens, which is too long considering the intended perioperative application. The results of the qualitative image evaluation, however, suggest that a condensed imaging protocol consisting of an HR TSE and a DW sequence may be sufficient to provide the required information for margin assessment. In this way, image acquisition may be reduced to around 15–20 min. In combination with estimated read times of around 15 min, or less as more experience is gained, this would yield a protocol that is achievable within a total time of approximately 30 min, which would be comparable to the time frame of FSA.³³ Although the present study did not yet fit with this time frame, we have shown proof of principle of obtaining high quality MR images from RLE specimens applicable for the assessment of surgical margins, which can be translated to a clinically realistic timeframe if a condensed imaging protocol is used. Third, the acquisition of the DW images was not time efficient. Faster imaging techniques, such as echo planar imaging (EPI), may be used instead of a DW-HASTE sequence. Hardware limitations of the MR machine used in this study, however, did not permit use of an EPI sequence. Furthermore, scanning time could be reduced by reducing the number of averages of the acquisition of the low *b*-values while maintaining them for the high *b*-values. Another option is to reduce the number of *b*-values used to calculate the ADC maps. While including more *b*-values provides a more accurate calculation of the ADC it also adds to the total scanning time. Before any changes to the DWI acquisition are made, the subsequent effects on the image quality should be investigated first. Finally, the ex vivo MRI was acquired using a costly 7 T scanner which is not widely available, therefore, our method should be reproduced on more readily available 1.5 T or 3 T clinical (whole-body) MRI systems to facilitate application in everyday clinical practice. However, switching from 7 T to lower field strengths might raise image quality issues in terms of signal to noise and scanning time. While increasing the scanning time is not a feasible option, we should investigate beforehand whether image quality would still be sufficient for surgical margin assessment, given the loss of signal to noise ratio as a result of using lower field strengths. Furthermore, using busy clinical systems can be logistically challenging. In our institution logistic challenges could be partly tackled by the clinical MRI system that we have available within the complex of operation theatres. Another option could be a dedicated (desktop/bench-top) ex vivo MRI system, but the requirement of a substantial initial investment is a disadvantage of this option.

The balance between tissue sparing and preventing LR is delicate. Current evidence on the optimal histological tumor-free margin is inconclusive. Several authors advocate 8 mm or greater histological tumor-free margins, as the risk for LR was up to twofold higher in patients with margins less than 8 mm compared with patients with margins of 8 mm or greater.^{15–18} Others, however, refute the minimal 8 mm histological margins by demonstrating barely any differences in LR rates between margins less than 8 mm and 8 mm or greater.^{35–37} Another ongoing discussion is the required surgical tumor-free margin to obtain 8 mm or greater tumor-free margins on final histology. While some recommend a surgical margin of 10 mm to compensate the formalin fixation induced shrinkage of 20–25%,^{15,17} others suggest a margin of 20 mm to compensate not only for tissue shrinkage but also for the discrepancy between the surgeon's estimation and the final histological tumor-free margin.^{6,19}

Ex vivo MRI of RLE specimens could provide perioperative information on the surgical tumor-free margins that could guide additional resection if necessary and prevent re-excision or adjuvant radiotherapy treatments. Furthermore, the technique could facilitate a less radical approach while maintaining control of LR by providing a more accurate measurement of the surgical margin than the surgeon's own estimation. If narrower histological margins are considered safe in the future, accurate perioperative measurements of the surgical margins will be even more important, as the estimation of a narrower surgical margin with the naked eye will become more difficult.

In conclusion, accurate localization of VSCC and measurements of the surgical tumor-free margins in fresh RLE specimens using ex vivo MRI seems feasible. High NPV and PPV for VSCC localization and identification of margins less than 8 mm suggest that ex vivo MRI is applicable in everyday clinical practice.

ACKNOWLEDGEMENT

Ex vivo MRI was performed using equipment of the Preclinical Imaging Centre (PRIME) within the Radboud University Medical Center, Nijmegen, The Netherlands.

FUNDING INFORMATION

This research was not supported by any grant. The authors have no financial relationship to disclose.

ABBREVIATIONS USED

ADC	apparent diffusion coefficient
AUC	area under the curve
CI	confidence interval
DSC	Dice similarity coefficient
DW	diffusion weighted
DWI	diffusion weighted imaging
EPI	echo planar imaging
FLASH	fast low-angle shot
FSA	frozen section analysis
HASTE	half-Fourier acquisition single-shot TSE
HR	high resolution
LR	local recurrence
NPV	negative predictive value
OCT	optical coherence tomography
PFPE	perfluoropolyether
PPV	positive predictive value
RLE	radical local excision
ROC	receiver operating characteristic
T1W	T ₁ weighted
T _E	echo time
T _R	repetition time
TSE	turbo spin echo
VSCC	vulvar squamous-cell carcinoma.

ORCID

Jan Heidkamp  <http://orcid.org/0000-0002-3335-1486>

REFERENCES

1. Siegel RL, Miller KD, Jemal A. Cancer statistics, 2016. *CA Cancer J Clin*. 2016;66(1):7-30.
2. Schuurman MS, Van Den Einden LCG, Massuger LFAG, Kiemeny LA, Van Der Aa MA, De Hullu JA. Trends in incidence and survival of Dutch women with vulvar squamous cell carcinoma. *Eur J Cancer*. 2013;49(18):3872-3880.
3. Lai J, Elleray R, Nordin A, et al. Vulvar cancer incidence, mortality and survival in England: age-related trends. *BJOG*. 2014;121(6):728-738.
4. Finan MA, Barre G. Bartholin's gland carcinoma, malignant melanoma and other rare tumours of the vulva. *Best Pract Res Clin Obstet Gynaecol*. 2003;17(4):609-633.
5. DiSaia PJ, Creasman WT. Invasive cancer of the vulva. In: Manning S, ed. *Clinical Gynecologic Oncology*. 4th ed. Saint Louis, MO: Mosby-Year Book; 1993:238-272.
6. de Hullu JA, van der Zee AGJ. Surgery and radiotherapy in vulvar cancer. *Crit Rev Oncol Hematol*. 2006;60(1):38-58.
7. Podratz KC, Symmonds RE, Taylor WF, Williams TJ. Carcinoma of the vulva: analysis of treatment and survival. *Obstet Gynecol*. 1983;61(1):63-74.
8. Carlson JW, Kauderer J, Walker JL, et al. A randomized phase III trial of VH fibrin sealant to reduce lymphedema after inguinal lymph node dissection: a Gynecologic Oncology Group study. *Gynecol Oncol*. 2008;110(1):76-82.
9. Andersen BL, Hacker NF. Psychosexual adjustment after vulvar surgery. *Obstet Gynecol*. 1983;62(4):457-462.
10. Aerts L, Enzlin P, Vergote I, Verhaeghe J, Poppe W, Amant F. Sexual, psychological, and relational functioning in women after surgical treatment for vulvar malignancy: a literature review. *J Sex Med*. 2012;9(2):361-371.
11. Ansink A, van der Velden J. Surgical interventions for early squamous cell carcinoma of the vulva. *Cochrane Database Syst Rev*. 2000;2:CD002036.
12. Stehman FB, Look KY. Carcinoma of the vulva. *Obstet Gynecol*. 2006;107(3):719-733.
13. Micheletti L, Preti M. Surgery of the vulva in vulvar cancer. *Best Pract Res Clin Obstet Gynaecol*. 2014;28(7):1074-1087.
14. Alkatout I, Schubert M, Garbrecht N, et al. Vulvar cancer: epidemiology, clinical presentation, and management options. *Int J Womens Health*. 2015;7:305-313.
15. Heaps JM, Fu YS, Montz FJ, Hacker NF, Berek JS. Surgical-pathologic variables predictive of local recurrence in squamous cell carcinoma of the vulva. *Gynecol Oncol*. 1990;38(3):309-314.

16. de Hullu JA, Hollema H, Lolkema S, et al. Vulvar carcinoma: the price of less radical surgery. *Cancer*. 2002;95(11):2331-2338.
17. Chan JK, Sugiyama V, Pham H, et al. Margin distance and other clinico-pathologic prognostic factors in vulvar carcinoma: a multivariate analysis. *Gynecol Oncol*. 2007;104:636-641.
18. Nooij LS, van der Slot MA, Dekkers OM, et al. Tumour-free margins in vulvar squamous cell carcinoma: does distance really matter? *Eur J Cancer*. 2016;65:139-149.
19. Palaia I, Bellati F, Calcagno M, Musella A, Perniola G, Panici PB. Invasive vulvar carcinoma and the question of the surgical margin. *Int J Gynaecol Obstet*. 2011;114(2):120-123.
20. Faul CM, Mirmow D, Huang Q, Gerszten K, Day R, Jones MW. Adjuvant radiation for vulvar carcinoma: improved local control. *Int J Radiat Oncol Biol Phys*. 1997;38(2):381-389.
21. Schueller-Weidekamm C, Schaefer-Prokop CM, Weber M, Herold CJ, Prokop M. CT angiography of pulmonary arteries to detect pulmonary embolism: improvement of vascular enhancement with low kilovoltage settings. *Radiology*. 2006;241(3):899-907.
22. Youden WJ. Index for rating diagnostic tests. *Cancer*. 1950;3(1):32-35.
23. Dice LR. Measures of the amount of ecologic association between species. *Ecology*. 1945;26(3):297-302.
24. Abe H, Shimauchi A, Fan X, et al. Comparing post-operative human breast specimen radiograph and MRI in lesion margin and volume assessment. *J Appl Clin Med Phys*. 2012;13(6):267-276.
25. Agresti R, Trecate G, Ferraris C, et al. Ex vivo MRI evaluation of breast tumors: a novel tool for verifying resection of nonpalpable only MRI detected lesions. *Breast J*. 2013;19(6):659-663.
26. Dashevsky BZ, D'Alfonso T, Sutton EJ, et al. The potential of high resolution magnetic resonance microscopy in the pathologic analysis of resected breast and lymph tissue. *Sci Rep*. 2015;5:17435.
27. Vandergugten S, Traore SY, Cartiaux O, Lecouvet F, Galant C, Docquier PL. MRI evaluation of resection margins in bone tumour surgery. *Sarcoma*. 2014;2014:967848.
28. Yamada I, Miyasaka N, Hikishima K, et al. Gastric carcinoma: ex vivo MR imaging at 7.0 T—correlation with histopathological findings. *Radiology*. 2015;275(3):841-848.
29. Yamada I, Miyasaka N, Hikishima K, et al. Ultra-high-resolution MR imaging of esophageal carcinoma at ultra-high field strength (7.0T) ex vivo: correlation with histopathologic findings. *Magn Reson Imaging*. 2015;33(4):413-419.
30. Steens SCA, Bekers EM, Weijs WLJ, et al. Evaluation of tongue squamous cell carcinoma resection margins using ex-vivo MR. *Int J Comput Assist Radiol Surg*. 2017;12(5):821-828.
31. Fan X, Haney CR, Agrawal G, et al. High-resolution MRI of excised human prostate specimens acquired with 9.4 T in detection and identification of cancers: validation of a technique. *J Magn Reson Imaging*. 2011;34(4):956-961.
32. Heidkamp J, Hoogenboom M, Kovacs IE, et al. Ex vivo MRI evaluation of prostate cancer: localization and margin status prediction of prostate cancer in fresh radical prostatectomy specimens. *J Magn Reson Imaging*. 2017;47(2):439-448.
33. Horn L-C, Wagner S. Frozen section analysis of vulvectomy specimens: results of a 5-year study period. *Int J Gynecol Pathol*. 2010;29(2):165-172.
34. Wessels R, van Beurden M, de Bruin DM, et al. The value of optical coherence tomography in determining surgical margins in squamous cell carcinoma of the vulva. *Int J Gynecol Cancer*. 2015;25(1):112-118.
35. Groenen SMA, Timmers PJ, Burger CW. Recurrence rate in vulvar carcinoma in relation to pathological margin distance. *Int J Gynecol Cancer*. 2010;20(5):869-873.
36. Woelber L, Kock L, Gieseck F, et al. Clinical management of primary vulvar cancer. *Eur J Cancer*. 2011;47(15):2315-2321.
37. Baiocchi G, Mantoan H, de Brot L, et al. How important is the pathological margin distance in vulvar cancer? *Eur J Surg Oncol*. 2015;41(12):1653-1658.

How to cite this article: Heidkamp J, Zusterzeel PLM, van Engen-van Grunsven ACH, et al. MRI evaluation of vulvar squamous-cell carcinoma in fresh radical local excision specimens for cancer localization and prediction of surgical tumor-free margins. *NMR in Biomedicine*. 2019;32:e4025. <https://doi.org/10.1002/nbm.4025>